REDSHIFTS OF THE BRIGHTEST X-RAY QSO's

A. K. SAPRE and V. D. MISHRA

Department of Physics, Ravishankar University, Raipur, India

(Received 13 March, 1985)

Abstract. The plot of the X-ray luminosity (in 0.5–4.5 KeV band and for Friedmann universe with $q_0 = +1$) of the brightest X-ray QSO at each redshift against redshift shows that the X-ray luminosity increases more or less monotonically with redshift upto $z \sim 3$. This result has been attributed to the selection effect known as the 'volume effect'. When this selection effect is taken into account in the optical, radio and X-ray windows of the electromagnetic spectrum, a sample of the brightest X-ray QSO's is obtained which shows a small dispersion in X-ray luminosity: $\langle \log L_{x_1} \rangle = 46.15 \pm 0.25$. The redshift–X-ray flux density plot for this sample gives slopes of both regression lines which agree, at a confidence level of 95% or greater, with the slopes expected theoretically if the redshifts of the QSO's are cosmological in nature.

1. Introduction

The Hubble diagram (i.e., the plot of redshift versus flux density) for quasi-stellar objects (QSO's) using corrected X-ray fluxes shows a large scatter (Sapre and Mishra, 1985). This implies that there is an apparent lack of correlation between redshift and X-ray flux density for QSO's. It is well known that the Hubble diagrams for QSO's using visual magnitudes and radio fluxes also exhibit a large scatter. Following the suggestion by McCrea (1972), a number of investigators – e.g., Bahcall and Hills (1973), Burbidge and O'Dell (1973), Usher (1975, 1978), Bahcall and Turner (1977), Kembhavi and Kulkarni (1977), Setti and Zamorani (1978), Pica and Smith (1983) – considered the magnitude-redshift relation for the optically brightest QSO's and obtained results consistent with the hypothesis that the redshifts of the QSO's are cosmological in nature, i.e., the QSO's are at the distances implied by their redshifts. In this paper we examine the Hubble diagram for the brightest X-ray QSO's taking into account the selection effects. This has been done in order to see whether the scatter in the Hubble diagram can be reduced and to test the validity of Hubble's law for the QSO's.

2. Data Analysis and Results

To examine the Hubble diagram for the brightest X-ray QSO's we have made use of the recently published data on X-ray luminosities of QSO's observed from Einstein observatory. Reichert *et al.* (1982) have published the data on X-ray luminosity, in 0.5–4.5 keV band corrected for galactic absorption, L_{x_0} (erg s^{-1} for Friedmann universe with deceleration parameter $q_0 = 0$ and $H_0 = 50$ km s^{-1} Mpc^{-1}) for a sample of 19 X-ray selected ('serendipitous') QSO's. Zamorani *et al.* (1981) have published the values of X-ray luminosity (L_{x_0}) for 107 previously known QSO's. However, out of these 107 QSO's, only 79 QSO's met the detection criteria. Chanan *et al.* (1981) have published the data on L_{x_0} for a sample of 19 X-ray selected ('serendipitous') QSO's.

Astrophysics and Space Science **115** (1985) 107–118. 0004–640X/85.15

While Grindlay *et al.* (1980) give the values of L_{x_0} for 6 X-ray selected ('serendipitous') QSO's, Ku *et al.* (1980) have published the data on L_{x_0} for a sample of 111 QSO's. Out of these, only 35 QSO's met the detection criteria. We have omitted the QSO 0100 + 0205 from our consideration because its redshift ($z = 1$) is reported to be uncertain. However, out of these 34 QSO's, 3 QSO's (viz., 1226 + 0220, 1703 + 6051, and 1704 + 6048) are already contained in the list of Zamorani *et al.* (1981) and, hence, we ignored them. Thus we have considered only 31 QSO's from the list of Ku *et al.* (1980). Tananbaum *et al.* (1979) give the data on L_{x_0} for a sample of 42 QSO's. However, out of these, 36 QSO's are already contained in the list of Zamorani *et al.* (1981) and Ku *et al.* (1980). Therefore, we have omitted these 36 QSO's. Thus we have considered only 6 QSO's from the list of Tanabaum *et al.* (1979). Henriksen *et al.* (1984) have published the data on L_{x_0} for a sample of 18 QSO's with known redshifts. Out of these, only 13 QSO's met the detection criteria. We have omitted 6 X-ray variable QSO's and 2 QSO's which Zamorani *et al.* (1981) give. Thus we have considered only 5 QSO's from Henriksen *et al.* (1984). Tananbaum *et al.* (1983) give the data on L_{x_0} for 33 QSO's. Out of these, 23 QSO's are already contained in Zamorani *et al.* (1981) and Ku *et al.* (1980). Therefore, we have considered a sample of only 10 QSO's from this list. It is thus seen that at present, a sample of 174 QSO's with positive X-ray detection in the fixed energy band of 0.5–4.5 keV at the source is available to us for statistical analysis. From the published values of L_{x_0} for the sample of 174 QSO's we have obtained the values of X-ray luminosity in 0.5–4.5 keV energy band, corrected for galactic absorption, L_{x_1} (erg s^{-1} for Friedmann cosmological model with $q_0 = 1$ and $H_0 = 50$ km s^{-1} Mpc^{-1}) by making use of the relation

$$\log L_{x_1} = \log L_{x_0} + \log \frac{4}{(2+z)^2} \,. \tag{1}$$

In Table I we have listed the values of the redshift (z), $\log(cz)$ together with the calculated values of X-ray luminosity (L_{x_1}), radio-luminosity (L_{R_1}) and the visual luminosity (L_{v_1}) for this sample of 174 QSO's.

If the redshift of QSO's are cosmological in nature, then for the Friedmann cosmological model with the deceleration parameter $q_0 = 1$, the Hubble diagram – i.e., the plot of $\log(cz)$ against corrected $\log f_x$ (erg s^{-1} cm^{-2}) – should produce a straight line of slope -0.5 for linear regression of $\log(cz)$ on $\log f_x$ and a straight line of slope -2.0 for linear regression of $\log f_x$ on $\log(cz)$. But the plot for the QSO's turns out to be a scatter diagram (Sapre and Mishra, 1985) having correlation coefficient of only 0.543. The slopes of both the regression lines are not consistent with the theoretically expected slopes at a confidence level of 95% or greater (see Table II). It the redshift of the QSO's are cosmological, then this large scatter must arise due to a large spread in the intrinsic luminosities of the QSO's:

$$\langle \log L_{x_1} \rangle = 44.99 \pm 0.77 \,.$$

As pointed out earlier, McCrea (1972) suggested that if this argument is valid, then the Hubble diagram for the brightest X-ray QSO's at each redshift should produce a statistically significant correlation.

TABLE I

Values of redshift, X-ray luminosity, radio luminosity, and visual luminosity for a sample of 174 X-ray QSO's

Coordinate designation of QSO	Redshift z	$\log(cz)$	X-ray luminosity (0.5–4.5 keV band) $\log L_{x_1}$ (erg s^{-1})	Radio luminosity (3.1–8.1 GHz band) $\log L_{R_1}$ (erg s^{-1})	Visual luminosity $\log L_{v_1}$ (erg s^{-1})
0351 + 026	0.036	4.033	43.18	–	43.69
0241 + 61	0.044	4.120	44.36	–	44.41
0037 + 061	0.063	4.276	43.37	–	43.86
1557 + 272	0.065	4.290	43.07	–	44.17
2251 – 1750	0.068	4.309	44.46	41.22	44.31
1219 + 755	0.070	4.322	44.43	41.04	44.96
0134 + 033	0.079	4.374	42.68	41.71	43.80
1704 + 607	0.080	4.380	42.57	–	43.82
1225.2 + 0858	0.085	4.406	43.83	–	44.24
1351 + 640	0.088	4.421	43.11	42.84	45.01
1059 + 730	0.089	4.426	43.66	–	45.09
1227 + 1403	0.100	4.477	43.72	–	44.08
1228.7 + 1219	0.116	4.541	43.94	–	44.32
1612 + 2612	0.131	4.594	44.47	42.90	45.12
1803 + 676	0.136	4.610	44.35	44.26	44.96
0026 + 129	0.142	4.629	44.84	42.08	45.44
1635 + 119	0.146	4.661	44.37	43.40	44.65
1055 + 605	0.149	4.650	44.25	–	44.59
1226.9 + 1336	0.150	4.653	43.67	–	44.50
1226 + 023** +	0.158	4.675	46.16	46.24	46.28
0919 + 515	0.161	4.684	44.03	–	44.31
2204 + 468	0.163	4.689	43.85	–	43.93
1701 + 610	0.164	4.692	44.03	–	44.70
1202 + 281	0.165	4.694	44.97	43.64	45.25
0054 + 144	0.171	4.710	44.68	42.26	44.83
1720 + 246	0.175	4.720	43.97	43.40	45.01
1028 + 313	0.177	4.725	44.87	44.04	44.86
1550 + 721	0.177	4.725	43.65	–	43.60
0210 + 860	0.184	4.742	43.67	45.09	44.05
0736 + 0143	0.191	4.758	44.36	45.14	45.30
0053 + 261 +	0.200	4.778	43.92	–	43.99
2135 – 147	0.200	4.778	45.15	44.95	45.44
2141 + 175*	0.213	4.805	44.11	44.53	45.56
0312 – 770	0.223	4.825	44.90	44.46	45.39
1510 + 390	0.228	4.835	44.11	–	44.14
1519 + 279	0.229	4.837	43.91	–	44.46
1525 + 1551	0.230	4.839	44.52	–	44.87
1217 + 023 +	0.240	4.857	45.31	44.64	45.16
2215 – 037	0.241	4.859	44.40	–	44.92
1328 + 315	0.241	4.859	44.07	–	44.57
0131 + 037	0.255	4.883	44.57	42.78	44.35
1545 + 2101 +	0.264	4.898	45.19	45.09	45.19
1339 + 053	0.266	4.902	44.39	–	45.14
1223 + 252	0.268	4.905	44.41	44.17	45.46
1246 + 335	0.271	4.910	44.21	43.23	44.74
2352 + 073	0.277	4.919	44.62	–	44.19
0031 – 076	0.291	4.941	44.28	–	44.77

Table I (continued)

Coordinate designation of QSO	Redshift z	$\log(cz)$	X-ray luminosity (0.5–4.5 keV band) $\log L_{x_1}$ (erg s^{-1})	Radio luminosity (3.1–8.1 GHz band) $\log L_{R_1}$ (erg s^{-1})	Visual luminosity $\log L_{v_1}$ (erg s^{-1})
1725 + 0429	0.293	4.944	44.00	45.03	44.78
2201 + 315*+	0.297	4.950	45.30	45.61	45.90
0845 + 378	0.307	4.964	44.08	–	44.85
1100 + 772*+	0.311	4.970	45.10	45.16	45.73
1250 + 5650	0.321	4.983	44.22	45.33	44.85
0137 – 010	0.330	4.995	44.75	43.41	45.45
2353 + 072	0.342	5.011	44.39	–	44.27
0150 – 102	0.361	5.034	44.36	–	44.87
1510 – 0854+	0.361	5.034	45.16	45.80	45.53
0130 + 033	0.363	5.037	44.77	43.51	45.30
0134 + 329*+	0.367	5.041	45.28	46.13	45.71
1704 + 608*	0.371	5.046	44.82	45.51	46.06
1058 + 7241	0.375	5.051	44.46	45.28	45.01
1612 + 2640	0.395	5.073	44.24	43.16	45.28
0137 + 060	0.396	5.075	44.14	43.32	45.39
2141 + 039	0.401	5.080	44.30	–	44.00
1430 + 625	0.402	5.081	44.35	–	44.69
0903 + 169+	0.411	5.091	44.99	45.16	44.95
0133 + 207+	0.425	5.105	45.55	45.59	45.03
1548 + 115+	0.436	5.116	45.29	45.02	45.48
1332 + 375	0.438	5.118	44.42	–	44.98
1526 + 285*	0.450	5.130	44.92	–	45.74
0844 + 377	0.451	5.131	44.62	–	45.25
0956 + 225	0.485	5.163	44.32	–	44.88
0438 – 1635	0.500	5.176	44.26	–	44.50
1847 + 335	0.509	5.184	44.90	–	45.51
0237 + 399	0.528	5.199	44.41	–	44.93
1258 – 055+	0.538	5.208	45.83	46.66	45.34
0538 + 498*	0.545	5.213	44.72	46.61	45.65
1618 + 177*+	0.555	5.221	45.11	45.62	45.92
0240 + 007*+	0.569	5.232	45.08	–	45.69
0830 + 1115*	0.589	5.247	44.68	44.33	45.58
1641 + 399*	0.594	5.251	44.37	–	44.82
1641 + 3954+	0.595	5.251	45.73	46.51	46.15
2345 – 1647+	0.600	5.255	45.01	45.97	45.31
1006 + 817*	0.630	5.276	44.73	–	46.16
1258 + 287	0.648	5.288	44.93	–	45.33
1258 + 2846	0.650	5.290	44.82	45.26	45.37
0637 – 75*+	0.651	5.290	46.12	46.49	46.36
1137 + 660*+	0.652	5.291	45.73	45.91	46.07
2344 + 092*+	0.677	5.307	45.52	45.90	46.23
0838 + 133+	0.684	5.312	45.20	45.92	45.42
1828 + 487*+	0.692	5.317	45.68	46.72	46.00
0923 + 392+	0.699	5.321	45.66	46.45	45.51
1224.7 + 093	0.731	5.341	44.48	–	45.17
2353 + 283*	0.731	5.341	44.91	–	45.60
1111 + 408+	0.734	5.343	45.42	45.93	45.48
1237 – 101*+	0.753	5.354	45.04	45.91	45.71

Table I (continued)

Coordinate designation of QSO	Redshift z	$\log(cz)$	X-ray luminosity (0.5–4.5 keV band) $\log L_{x_1}$ (erg s^{-1})	Radio luminosity (3.1–8.1 GHz band) $\log L_{R_1}$ (erg s^{-1})	Visual luminosity $\log L_{v_1}$ (erg s^{-1})
0518 + 165 +	0.760	5.358	45.12	46.54	45.46
0710 + 118* +	0.768	5.362	45.06	45.83	46.40
1623 + 2657*	0.779	5.368	44.87	45.65	45.74
0414 – 060* +	0.781	5.369	45.60	45.52	46.76
1726 + 499	0.815	5.388	44.80	–	45.08
1806 + 456	0.830	5.396	44.67	–	45.13
1328 + 307* +	0.849	5.406	45.09	46.92	45.88
0440 – 0023 +	0.850	5.406	45.51	46.30	45.17
0336 – 019 +	0.852	5.407	45.12	46.67	45.45
2251 + 158** +	0.859	5.411	45.99	46.95	46.39
0809 + 483*	0.871	5.417	44.97	46.77	45.74
1252 + 119* +	0.871	5.417	45.45	45.91	46.15
1422 + 202* +	0.871	5.417	45.20	45.94	45.66
0537 – 441* +	0.894	5.428	45.47	46.51	46.68
2216 – 0350* +	0.901	5.432	45.48	45.96	46.30
1458 + 718* +	0.905	5.433	45.55	46.64	46.15
0420 – 0127* +	0.915	5.438	45.79	46.25	45.79
1622 + 238* +	0.927	5.444	45.08	46.08	45.89
1555 + 33*	0.942	5.451	44.81	45.14	45.56
1340 + 606*	0.961	5.460	44.77	45.90	45.64
1206 – 399* +	0.966	5.462	45.29	45.75	46.20
0237 + 04 +	0.978	5.467	45.16	45.88	45.51
1435 + 2452 +	1.010	5.481	45.09	45.60	45.32
0906 + 0133* +	1.018	5.485	45.49	46.23	45.99
1040 + 123* +	1.029	5.489	45.50	46.37	46.03
2230 + 114** +	1.037	5.493	45.96	46.74	46.04
1328 + 254* +	1.055	5.500	45.35	46.74	45.88
0740 + 380* +	1.063	5.503	45.40	45.84	46.00
0850 + 140* +	1.110	5.522	45.39	46.21	46.07
0833 + 654* +	1.112	5.523	45.49	45.83	45.75
1524 + 101* +	1.358	5.610	45.24	45.38	45.95
0112 – 017* +	1.365	5.612	45.66	46.26	46.18
1258 + 2837 +	1.373	5.614	45.26	45.23	45.54
1739 + 522* +	1.375	5.615	45.70	46.75	45.81
0302 – 223* +	1.400	5.623	45.44	–	46.77
2223 – 052** +	1.404	5.624	46.52	46.87	45.82
1416 + 067* +	1.436	5.634	45.57	46.81	46.47
0835 + 580* +	1.534	5.663	45.50	46.47	46.23
1711 + 7116* +	1.600	5.681	45.02	–	46.31
1011 + 2504* +	1.631	5.689	46.08	45.89	47.12
1556 + 335* +	1.650	5.694	45.30	45.58	46.50
2037 + 5108* +	1.686	5.704	45.59	–	45.65
0954 + 495* +	1.687	5.704	45.58	–	45.63
1318 + 290* +	1.703	5.708	45.61	44.40	46.54
2120 + 168* +	1.805	5.733	45.15	46.43	46.27
1633 + 3814* +	1.814	5.735	45.67	46.68	46.18
2121 + 0522** +	1.878	5.751	45.87	46.53	46.45
0802 + 103* +	1.956	5.768	45.56	46.64	46.17

Table I (continued)

Coordinate designation of QSO	Redshift z	$\log(cz)$	X-ray luminosity (0.5–4.5 keV band) $\log L_{x_1}$ (erg s^{-1})	Radio luminosity (3.1–8.1 GHz band) $\log L_{R_1}$ (erg s^{-1})	Visual luminosity $\log L_{v_1}$ (erg s^{-1})
0438 – 1638*+	1.960	5.769	45.49	–	46.33
1703.5 + 609*+	1.980	5.773	45.78	45.68	46.46
1606 + 2857*+	1.989	5.775	45.10	46.21	45.84
1704 + 7101*	2.000	5.778	44.89	–	46.47
0848 + 1533*+	2.010	5.780	45.42	46.12	46.40
0017 + 154*+	2.012	5.780	45.34	46.63	46.16
0226 – 038*+	2.064	5.792	45.94	46.32	46.67
2357 – 348*+	2.070	5.793	45.64	45.82	46.64
1331 + 170*+	2.081	5.795	45.72	45.84	47.05
2254 + 024*+	2.090	5.797	45.37	46.04	46.27
1054 – 034*	2.100	5.799	44.96	45.62	46.28
0106 + 0119**+	2.107	5.800	46.04	46.85	46.11
0043 + 008*+	2.150	5.809	45.75	45.86	46.68
0424 – 131*+	2.165	5.812	45.32	46.44	46.52
1309 – 056*+	2.180	5.815	45.81	45.11	46.69
0237 – 2322**+	2.223	5.824	46.51	47.31	46.85
1225 – 317*+	2.230	5.825	46.03	45.91	47.15
0458 – 02*+	2.286	5.836	45.53	46.82	46.25
0205 – 379*+	2.420	5.861	45.59	45.31	46.68
1623 + 2653*+	2.480	5.871	45.21	44.50	46.40
0528 – 250*+	2.765	5.919	46.23	46.73	46.65
0207 – 398*+	2.805	5.925	45.67	45.18	46.66
0438 – 436*+	2.852	5.932	46.09	47.44	46.19
0805 + 0441*+	2.877	5.936	45.88	46.50	46.56
0537 – 286*+	3.110	5.970	46.39	46.54	45.82
0420 – 388*+	3.120	5.971	46.03	46.13	47.00
2204 – 608*+	3.180	5.979	45.68	45.43	46.76
1402 + 044*+	3.202	5.982	45.43	46.47	46.36
2126 – 150*+	3.270	5.991	46.92	46.73	46.88
0642 + 449*+	3.402	6.009	46.34	47.10	46.56
1442 + 1011*+	3.530	6.025	46.18	47.18	46.72

* These QSO's are free from the optical selection effect and can be detected up to $z = 3.53$.
\+ These QSO's are free from the X-ray selection effect and can be detected up to $z = 3.53$.
*+ These QSO's are free from the optical, radio, and X-ray selection effects and can be detected up to $z = 3.53$.
**+ These QSO's are the brightest QSO's in each redshift bin and free from the optical, radio, and X-ray selection effects (see text).

To plot the Hubble diagram for the brightest X-ray QSO's, we have arranged the sample of 174 QSO's in ascending order of redshifts and have divided the redshift range into 17 bins, each bin containing 10 QSO's. The plot of $\log L_{x_1}$ for the brightest X-ray QSO's in each bin against average logarithm of the redshift of the QSO's in that bin, $\langle \log cz \rangle$ (c = 299792.456 km s^{-1} is the speed of light in vacuum), is shown in Figure 1. It is seen that the X-ray luminosity of the 17 brightest X-ray QSO increases more or less monotonically with redshift up to $z \sim 3$. This behaviour seems to be quite different

TABLE II

Results of the linear regression analyses of $[\log(cz), \log f_x]$ pairs for various samples of X-ray QSO's

Sample	No. of QSO's	Slope A A'	Standard deviation in slope σ_A $\sigma_{A'}$	Correlation coefficient Y	$t_A = \frac{A-(-0.5)}{A}$ $t_{A'} = \frac{A'-(-2.0)}{A'}$	Significance level 0.05	0.01	$\langle \log L_{x_1} \rangle$ $\sigma \log L_{x_1}$
(1)	(2)	(3)	(4)	(5)	(6)	(7)		(8)
All QSO's	174	−0.454 −0.649 (b)	±0.004 ±0.006 (b)	0.543 (b)	11.355 231.567 (b)	Yes Yes	Yes Yes (b)	44.99 0.77 (b)
Sample A	17	−0.639 −1.042	±0.300 ±0.049	0.816	4.596 19.458	Yes Yes	Yes Yes	45.75 0.54
Sample B	9	−0.483 −1.419	±0.047 ±0.137	0.828	0.370 4.225	No Yes	No Yes	46.24 0.31
Sample C	7	−0.435 −1.753	±0.049 ±0.195	0.874	1.333 1.264	No No	No No	46.15 0.25

In columns 3, 4, and 6, upper values for each sample of QSO's correspond to linear regression of $\log(cz)$ on $\log f_x$ whereas the lower values correspond to linear regression of $\log f_x$ on $\log(cz)$. Sample A: brightest X-ray QSO's in 17 redshift bins. Sample B: brightest X-ray QSO's with optical selection effect removed. Sample C: brightest X-ray QSO's with optical, radio, and X-ray selection effects removed.

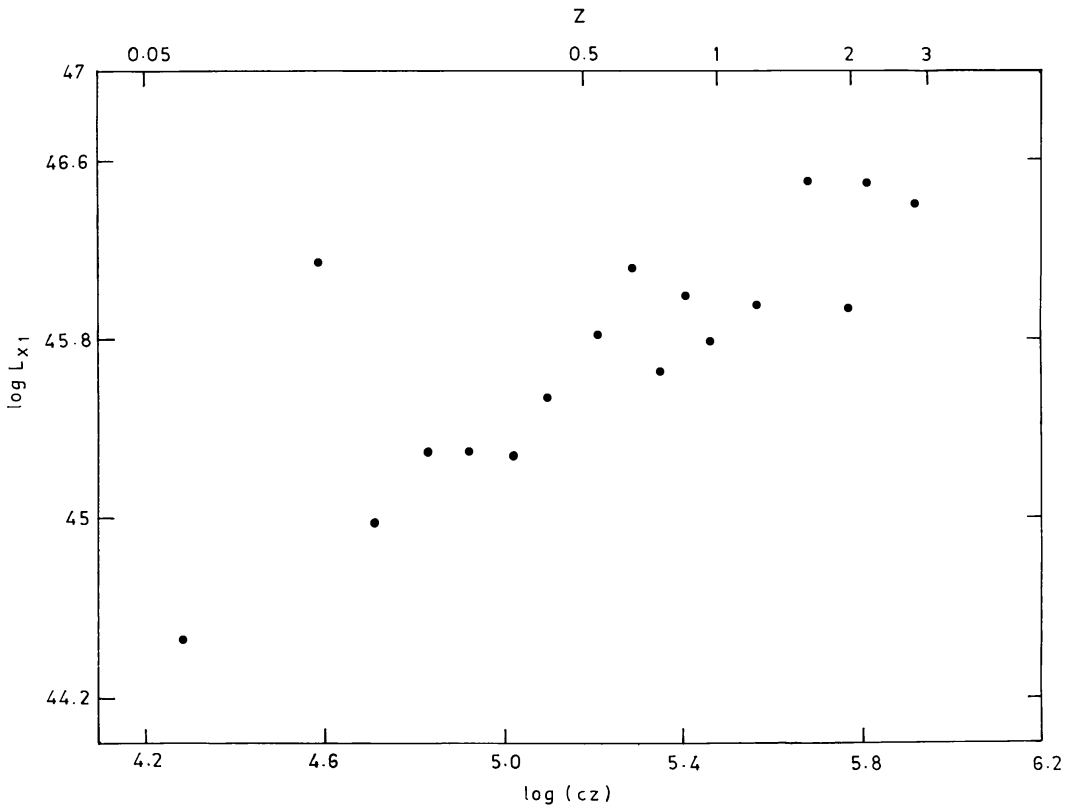

Fig. 1. Plot of $\log L_{x_1}$ against $\langle \log(cz) \rangle$ for the brightest X-ray QSO's in each of 17 redshift bins. For this sample, $\langle \log L_{x_1} \rangle = 45.75 \pm 0.54$.

from that of the brightest optical QSO's found by Kembhavi and Kulkarni (1977) in which the absolute visual magnitude of the brightest QSO's increases with redshift up to $z \sim 1$, after which it remains nearly constant up to $z \sim 3.5$. The behaviour seen in Figure 1 is clearly due to the selection effect known as 'volume effect'. Since intrinsically very bright X-ray QSO's are expected to be rare, one has to sample larger and larger volume of space (i.e., larger z) to detect them. The brightest X-ray QSO's seem to have larger spread in X-ray luminosity as compared to the optically brightest QSO's. Due to this selection effect one detects a large number of intrinsically less bright X-ray QSO's at smaller redshifts and a large number of intrinsically more bright X-ray QSO's at larger redshifts, because intrinsically less bright X-ray QSO's would be below the observational X-ray cut-off at larger redshifts. This bias leads to the larger value for the slope $|A| = 0.639$ of linear regression of $\log(cz)$ on $\log f_x$ than the slope of 0.5 expected theoretically if the redshift of the QSO's are cosmological in nature. Similarly the slope of $|A'| = 1.042$ for linear regression of $\log f_x$ on $\log(cz)$ turns out to be smaller than the theoretically expected slope of 2.0. Although the correlation coefficient for the sample of 17 brightest X-ray QSO's has increased to 0.816 the t-statistic shows that the departure of the slopes of both the linear regression lines from the theoretically expected ones is significant at 0.05 and 0.01 levels of significance (see Table II). Further, this sample A of 17 brightest X-ray QSO's has considerable scatter in X-ray luminosity given by $\langle \log L_{x_1} \rangle = 45.75 \pm 0.54$.

To remove this selection effect one should consider only those QSO's which can be detected, in the appropriate optical, radio, and X-ray bands at all redshifts up to $z = 3.53$ – the largest redshift at which the QSO's have been detected in these bands. This is because optical, radio, and X-ray emissions from QSO's might be correlated (Zamorani *et al.*, 1981) and QSO's in each of these bands suffer from the volume selection effect. To allow for the optical selection effect we have considered only those QSO's, following Burbidge and O'Dell (1973), which lie to the brighter side of the line $\log(cz) = 0.2\, m_v + 1.729$. The values of the redshift and visual magnitude m_v have been taken from Hewitt and Burbidge (1980). The galactic absorption correction and K-correction are applied to m_v as described in Thakur and Sapre (1978). This procedure ensures that for the optical detectability limit $m_v = 21.48$, all QSO's lying to the brighter side of the line would be visible at all redshifts up to $z = 3.53$. We are then left with a sample of 90 X-ray QSO's free from the optical selection effect. It turns out that this sample contains most of the radio QSO's which can be detected at all redshifts up to 3.53 if the radio detectability limit is put at $\log f_r = -12.65$ (see Table I; corrected radio fluxes f_r have been calculated for the 3.1–8.1 GHz band at the source from published 1.4 GHz fluxes and spectral indices following the prescription given by Schmidt, 1968). Hence, we have not applied the radio selection effect to this sample. This sample gives rise to 9 redshift bins, each bin containing 10 QSO's. For this sample B which is free from the optical and radio selection effects, the scatter in X-ray luminosity has decreased considerably: $\langle \log L_{x_1} \rangle = 46.24 \pm 0.31$. Figure 2, which depicts the plot of $\log L_{x_1}$ against $\langle \log(cz) \rangle$ for this sample, shows that the X-ray luminosity of the brightest X-ray QSO's remains nearly constant up to $z \sim 2$. The Hubble plot for the brightest X-ray

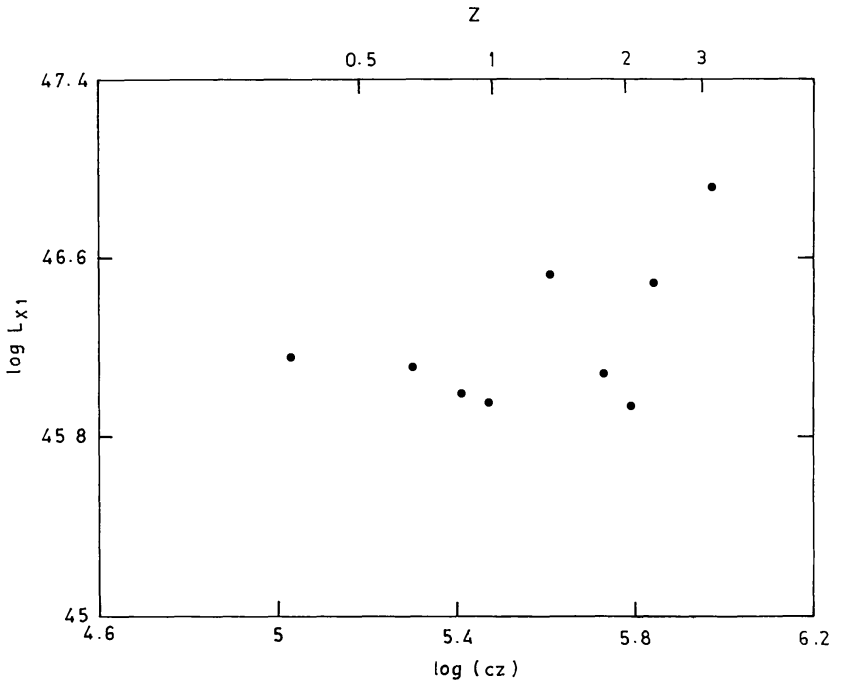

Fig. 2. Plot of $\log L_{x_1}$ against $\langle \log(cz) \rangle$ for the brightest X-ray QSO's obtained after removing the optical selection effect (see text). For this sample, $\langle \log L_{x_1} \rangle = 46.24 \pm 0.31$.

QSO's in this sample shows that the value of the correlation coefficient has improved to $r = 0.828$ and the slope of the least-squares linear regression of $\log(cz)$ on $\log f_x$ has improved to $A = -0.483 \pm 0.047$ consistent with the theoretically expected slope of $A = -0.5$. The agreement between the two values is significant at a confidence level of

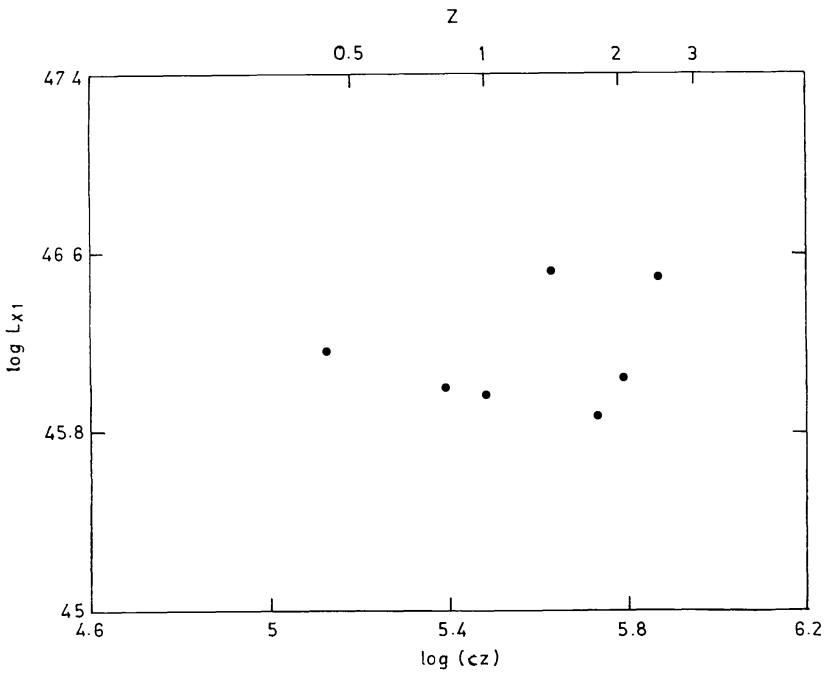

Fig. 3. Plot of $\log L_{x_1}$ against $\langle \log(cz) \rangle$ for the brightest QSO's obtained after removing the optical, radio, and X-ray selection effects (see text). For this sample, $\langle \log L_{x_1} \rangle = 46.15 \pm 0.25$.

95% or greater. However, the depature of the slope of the linear regression of $\log f_x$ on $\log(cz)$ ($A' = -1.419 \pm 0.137$) from the theoretically expected slope of $A' = -2.0$ is still significant at a significance level of 0.05 and 0.01 (see Table II). This shows that the sample is still biased towards fainter X-ray fluxes. To avoid the X-ray selection effect, we have considered only those QSO's from the sample of 174 objects that lie to the brighter side of the line $\log(cz) = -0.5 \log f_x - 0.846$. We are then left with a sample of 95 QSO's which can be detected at all redshifts up to $z = 3.53$ if the X-ray detectability limit is put at $\log f_x = -13.74$. We have then considered those QSO's which are common to this sample and the sample *B*. The resulting sample consists of 77 QSO's which is free from the optical, radio, and X-ray selection effects (see Table I). These QSO's fall into seven complete redshift bins, each bin containing 10 QSO's. This sample *C* has a small dispersion in X-ray luminosity: $\langle \log L_{x_1} \rangle = 46.15 \pm 0.25$. Figure 3 shows a plot of $\log L_{x_1}$ against $\langle \log(cz) \rangle$ for this sample. It is seen that the X-ray luminosity of the brightest QSO's in this sample remains substantially constant at all redshifts up to $z \sim 3$. The Hubble plot for the brightest X-ray QSO's in this sample shows a further

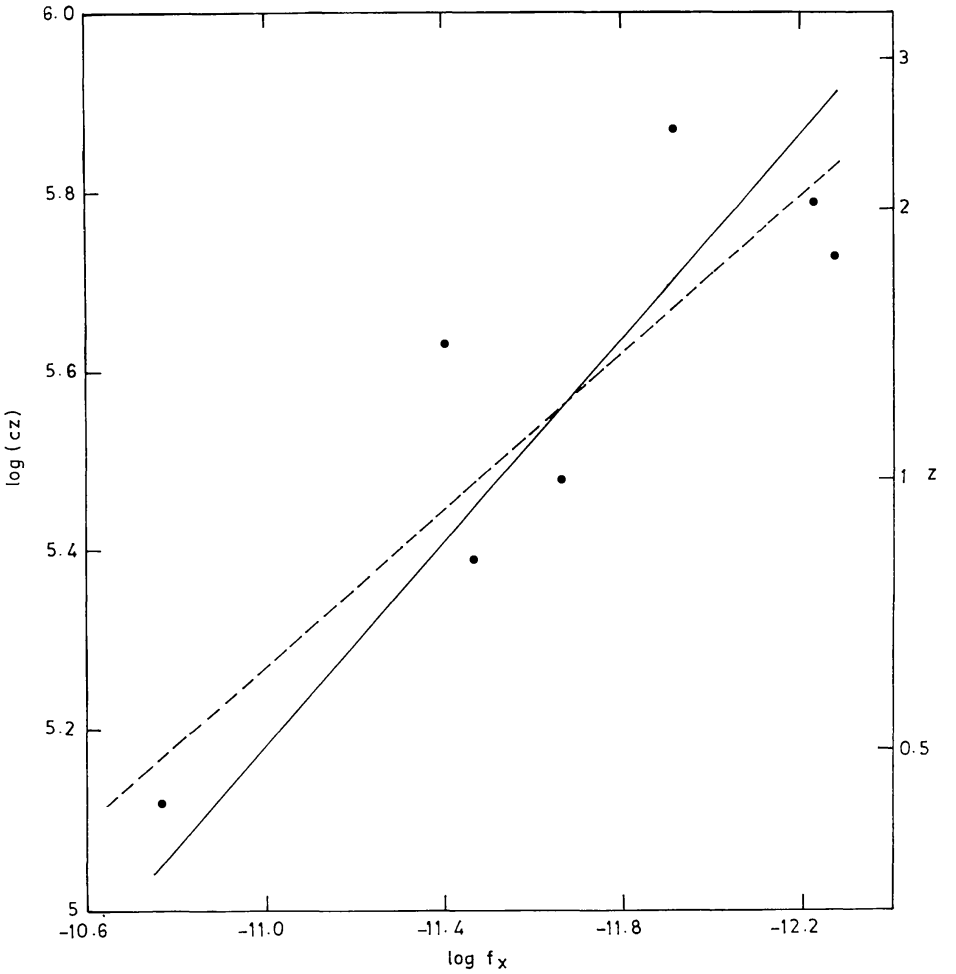

Fig. 4. Plot of $\langle \log(cz) \rangle$ against $\log f_x$ for the brightest X-ray QSO's free from the optical, radio, and X-ray selection effects. The continuous line represents the linear regression of $\log(cz)$ on $\log(f_x)$ whereas the dotted line corresponds to the linear regression of $\log(f_x)$ on $\log(cz)$.

improvement in the correlation coefficient: $r = 0.874$. The slope of the linear regression of $\log(cz)$ on $\log f_x$ for this sample turns out to be $A = -0.435 \pm 0.049$. The slope of te linear regression of $\log f_x$ on $\log(cz)$ turns out to be $A' = -1.753 \pm 0.195$ (see Table II). Figure 4 shows the Hubble plot for this sample together with the two regression lines. The t-statistic shows that the departure of the slopes A and A' of the two regression lines from the theoretically expected slopes of -0.5 and -2.0, respectively, is not significant at a significance level of 0.05 and 0.01. This sample, therefore, behaves as an unbiased standard candle in X-ray luminosity in 0.5–4.5 keV band at the source and it covers almost the entire redshift range of the QSO's. These QSO's have been marked with an asterisk (**) in Table I.

3. Discussion

The scatter in the X-ray Hubble diagram of QSO's arises mainly due to the large spread in the intrinsic X-ray luminosity and X-ray variability of QSO's. To avoid the scatter due to X-ray variability we have considered only those QSO's which do not exhibit X-ray variability, although X-ray variability of $\Delta \log f_x > 0.3$ in QSO's is rather rare (Zamorani *et al.*, 1984). Then the scatter and the apparent lack of redshift-flux density correlation arises due to the volume selection effects. If the volume selection effects in the optical, radio, and X-ray regions are taken into account as explained in Section 2, we obtain a sample of 7 brightest X-ray QSO's which shows a significant redshift-flux density correlation and considerably small dispersion in X-ray luminosity and redshift. As a result, we obtain the slopes of both the regression lines consistent with those expected if the QSO's are at the distances implied by their redshifts, thus supporting the cosmological nature of their redshifts.

Acknowledgement

One of us (VDM) would like to thank Professor R. K. Thakur for offering the facilities to work in the Physics Department of the Ravishankar University, Raipur (M.P.).

References

Bahcall, J. N. and Hills, R. E.: 1973, *Astrophys. J.* **179**, 699.
Bahcall, J. N. and Turner, E. L.: 1977, in D. L. Jauncey (ed.), 'Radio-Astronomy and Cosmology', *IAU Symp.* **74**, 295.
Burbidge, G. R. and O'Dell, S. L.: 1973, *Astrophys. J.* **183**, 759.
Chanan, G. A., Margon, B., and Downes, R. A.: 1981, *Astrophys. J.* **243**, L5.
Grindlay, J. E., Steiner, J. E., Forman, W. R., Canizares, C. R., and McClintock, J. E.: 1980, *Astrophys. J.* **239**, L43.
Henriksen, M. J., Marshall, F. E., and Mushotzky, R. F.: 1984, *Astrophys. J.* **284**, 491.
Hewitt, A. and Burbidge, G. R.: 1980, *Astrophys. J. Suppl. Ser.* **43**, 57.
Kembhavi, A. K. and Kulkarni, V. K.: 1977, *Monthly Notices Roy. Astron. Soc.* **181**, 19.
Ku, W. H. M., Helfand, D. J., and Lucy, L. B.: 1980, *Nature* **288**, 323.
McCrea, W. H.: 1972, in D. S. Evans (ed.), 'External Galaxies and Quasi-Stellar Objects', *IAU Symp.* **44**, 283.

Pica, A. J. and Smith, A. G.: 1983, *Astrophys. J.* **272**, 11.
Reichert, G. A., Mason, K. O., Thorstensen, F. R., and Bowyer, S.: 1982, *Astrophys. J.* **260**, 437.
Sapre, A. K. and Mishra, V. D.: 1985, *J. Astrophys. Astron.* **6**, 49.
Schmidt, M.: 1968, *Astrophys. J.* **151**, 393.
Setti, G. and Zamorani, G.: 1978, *Astron. Astrophys.* **66**, 249.
Tananbaum, H., Avni, Y., Branduardi, G., Elvis, M., Fobbiano, G., Feigelson, E., Giacconi, R., Henry, J. P., Pye, J. P., Soltan, A., and Zamorani, G.: 1979, *Astrophys. J.* **234**, L9.
Tananbaum, H., Wardle, J. F. C., Zamorani, G., and Avni, Y.: 1983, *Astrophys. J.* **268**, 60.
Thakur, R. K. and Sapre, A. K.: 1978, *Astrophys. Space Sci.* **57**, 119.
Usher, P. D.: 1975, *Astrophys. J.* **198**, L57.
Usher, P. D.: 1978, *Astrophys. J.* **222**, 40.
Zamorani, G., Giommi, P., Maccacaro, T., and Tananbaum, H.: 1984, *Astrophys. J.* **278**, 28.
Zamorani, G., Henry, J. P., Maccacaro, T., Tananbaum, H., Soltan, A., Leibert, J., Stocke, J., Strittmatter, P. A., Weymann, R. J., Smith, M. G., and Condon, J. J.: 1981, *Astrophys. J.* **245**, 357.